Influence of flexoelectric effect on the Fréedericksz transition in chiral nematic liquid crystals

A. D. Oskirko* and S. V. Ul'yanov†
Department of Physics, St. Petersburg State University, 7/9 Universitetskaya Emb., St. Petersburg 199034, Russia

A. Yu. Val'kov‡
Department of Mathematics, Peter the Great St. Petersburg Polytechnic University, St. Petersburg 195251, Russia

(Received 8 January 2018; revised manuscript received 6 June 2018; published 23 July 2018)

Electric field driven Frèedericksz transition in chiral nematic (cholesteric) planar liquid crystal cell is studied in the presence of flexoelectric effect. An inhomogeneity of electric field and finiteness of anchoring energy are considered. The extra contribution to the electric field induced by flexoelectricity is taken into account as well as the common contribution arising from the applied voltage U. Equilibrium director distribution is obtained in dependence on voltage and flexoelectric coefficients by numerical minimization of the free energy. The threshold voltage was found to decrease with the increase of the flexoelectric coefficients within the range of high flexoelectric coefficients. Thus flexoelectricity promotes the transition. The orientational structure becomes asymmetric about the center of the cell due to flexoelectricity, even in the case of symmetric boundary conditions. The equilibrium structure was also shown to be different for $U > 0$ and $U < 0$. It was found, that for sufficiently high flexoelectric coefficients the director distribution can be described by a simple function. In this case the planar helicoidal structure transfers into a hybrid-aligned one as the voltage increases. This transformation may form the basis for new flexoelectricity-based switching devices. The nonmonotonic behavior of threshold voltage can be observed in the case of small flexoelectric coefficients. An analytical form of the stability conditions was obtained for the planar helicoidal configuration. We have shown that the Frèedericksz transition can be either continuous or discontinuous depending on the material constants and thickness of the liquid crystal cell.

DOI: 10.1103/PhysRevE.98.012702

I. INTRODUCTION

Molecular reorientation effect in the liquid crystal (LC) cells induced by an external field attracts attention of researchers due to its applications. This phenomenon known as the Fréedericksz transition (effect) was discovered in the end of 1920's. Among the devices based on the Fréedericksz transition, we can point to LC displays, switchable diffraction gratings, mirrorless lasers, and others [1]. The Fréedericksz transition was studied for different types of inducing fields: static electric and magnetic fields, oscillating electric field, laser radiation; and for different types of LC phases: nematics, cholesterics, smectics, etc. [2–4].

The simplest way of accounting for anchoring effects in the Fréedericksz transition is to use rigid boundary conditions. Weak anchoring is usually described by the Rapini-Popular potential [5]. It is important to note that theory of the Fréedericksz transition in electric and magnetic fields is quite different, due to the spatial inhomogeneity of the electric field inside the LC cell [6–10]. The Fréedericksz transition in nematics has earlier been treated as an orientational phase transition of the second order [11], i.e., the continuous phase transition. However, in chiral nematics (cholesterics) it turns to be either continuous or discontinuous depending on the material constants [12].

Recently, there has been observed growing interest in studying the influence of flexoelectricity [13] on threshold effects in liquid crystals, e.g., switching in bistable nematic LC devices [14–16]. Flexoelectricity provides additional distortions to the electric field, thus it also affects the Fréedericksz transition. Such transition in a nematic LC was studied in [17–19]. The analysis was restricted to the rigid boundary conditions and to the lowest harmonic approximation for the director and for the electric field spatial distributions.

In this work the Fréedericksz transition for a static electric field in the plane-parallel cholesteric LC cell is investigated theoretically accounting for the flexoelectric effect, finite surface anchoring energy, and spatial inhomogeneity of the electric field. Three issues are in the focus of our attention: the threshold voltages, the director configuration above the threshold, and the type of the orientational transition. Special emphasis is given to the stability of equilibrium structures and to phase diagrams.

The paper is organized as follows. In Sec. II the free energy functional of a plane-parallel LC cell is derived as a sum of bulk and surface inputs. The bulk free energy includes elastic, electric field, and flexoelectric terms. Electric field spatial inhomogeneity induced by dielectric anisotropy and by flexoelectricity is taken into consideration. The surface free energy is described with the Rapini-Papoular–type potential. In Sec. III the equilibrium spatial distribution of the director is found for a wide range of material parameters. The phase diagrams, including stability and metastability zones, are found using the numerical variation analysis. In Sec. IV the stability

*antonimus@protonmail.ch
†ulyanov_sv@mail.ru
‡Department of Physics, St. Petersburg State University, 7/9 Universitetskaya Emb., St. Petersburg, 199034, Russia; alexvalk@mail.ru

of the planar helicoidal structure is studied analytically. In Sec. V the type of the Fréedericksz transition (continuous or discontinuous) is analyzed within the two-parametric Landau-type model. Section VI contains summary and discussions.

II. DISTORTION FREE ENERGY

We consider a chiral nematic liquid crystal contained between two parallel flat electrodes with a weak surface anchoring. Consider that the liquid crystal occupies the layer $0 \leqslant z \leqslant L$ with the z axis directed normally to the boundaries. The system is assumed to be homogeneous in x, y directions; in particular, the director $\mathbf{n}(\mathbf{r}) = \mathbf{n}(z)$, thus excluding from the consideration the Helfrich-type instabilities [3] and the edge effects. We parametrize the director $\mathbf{n}$ in the form

$$n_x = \sin\theta\cos\varphi,\ n_y = \sin\theta\sin\varphi,\ n_z = \cos\theta, \tag{2.1}$$

with polar and azimuthal angles θ and φ, respectively.

The distortion free energy of a chiral nematic cell can be expressed as a sum of three terms:

$$\mathcal{F}_{\rm tot} = \mathcal{F}_e + \mathcal{F}_{\rm sf} + \mathcal{F}_f. \tag{2.2}$$

The first term presents the Oseen-Frank elastic energy [3]:

$$\mathcal{F}_e = \frac{S_\perp}{2}\int_0^L [K_{11}(\operatorname{div}\mathbf{n})^2 + K_{22}(\mathbf{n}\cdot\operatorname{curl}\mathbf{n} + q_0)^2 + K_{33}(\mathbf{n}\times\operatorname{curl}\mathbf{n})^2]\,dz, \tag{2.3}$$

where $S_\perp$ is the area of boundary plates, K_{ii} are the Frank constants, π/q_0 is the helix period (half of the helix pitch). Inserting Eq. (2.1) into (2.3), we obtain

$$\mathcal{F}_e = \mathcal{F}_e^{(0)} + \frac{S_\perp}{2}\int_0^L [A(\theta)\theta'^2 + B(\theta)\varphi'^2 - 2C(\theta)\varphi']dz, \tag{2.4}$$

$$\begin{aligned} A(\theta) &= K_{11}\sin^2\theta + K_{33}\cos^2\theta,\\ B(\theta) &= \sin^2\theta(K_{22}\sin^2\theta + K_{33}\cos^2\theta),\\ C(\theta) &= q_0 K_{22}\sin^2\theta, \end{aligned} \tag{2.5}$$

where $\mathcal{F}_e^{(0)} = VK_{22}q_0^2/2$, and $V = S_\perp L$ is the volume of the cell; the prime denotes the derivative with respect to z.

In Eq. (2.3) there should exist extra surfacelike terms

$$\mathcal{F}_{13} = K_{13}\int_V \operatorname{div}(\mathbf{n}\operatorname{div}\mathbf{n})d\mathbf{r},$$

$$\mathcal{F}_{24} = -\frac{K_{22}+K_{24}}{2}\int_V \operatorname{div}(\mathbf{n}\operatorname{div}\mathbf{n} + \mathbf{n}\times\operatorname{curl}\mathbf{n})d\mathbf{r},$$

where K_{13} and K_{24} are the splay-bend and the saddle-splay modules [20,21]. In the case of $\mathbf{n} = \mathbf{n}(z)$ we obtain [21]

$$\mathcal{F}_{13} = -\tfrac{1}{2}S_\perp K_{13}\theta'\sin 2\theta\Big|_0^L,\ \mathcal{F}_{24} = 0.$$

Note that $K_{22} + K_{24} = 0$ in chiral nematics, according to [4]. The LC elastic free energy occurs to be unbounded from below due to $\mathcal{F}_{13}$ term, producing the so-called Oldano-Barbero paradox [22]. There are several principal ways of solving this problem [20,21,23]. The first one is based on a modification of the volume and/or the surface elastic free energy. The second one involves deriving the equality $K_{13} = 0$. The latter relation has been obtained in some of the LC molecular models as well as in a continuous medium approach. The third approach asserts that the first derivatives of the director at the boundaries obey the bulk equilibrium equations, hence, $\theta'(0)$ and $\theta'(L)$ are not free parameters. In fact, the K_{13} problem is still cyclically closing-unclosing. In this work, in what follows we omit $\mathcal{F}_{13}$ term as it is usually done in analysis of the Fréedericksz transition.

The second term in Eq. (2.2) presents the surface anchoring energy. We approximate it as

$$\mathcal{F}_{\rm sf} = \frac{S_\perp}{2}\sum_{\alpha=1,2}\left[W_\theta^{(\alpha)}\sin^2\left(\theta-\theta_0^{(\alpha)}\right) + W_\varphi^{(\alpha)}\sin^2\left(\varphi-\varphi_0^{(\alpha)}\right)\right].$$

Here, $\alpha = 1, 2$ correspond to the boundaries $z = 0, L$, respectively. Constants $W_{\theta,\varphi}^{(\alpha)} > 0$ are the elastic modules of the surface anchoring energy, and the angles $\theta_0^{(\alpha)}$ and $\varphi_0^{(\alpha)}$ describe the easy directions at the boundaries. This formula is an anisotropic version of Rapini-Papoular potential [5]. Rigid boundary conditions correspond to the limit $W_{\theta,\varphi}^{(\alpha)} \to \infty$.

The third term arises due to the external electric field

$$\mathcal{F}_f = \int_V F_f\,d\mathbf{r},\ F_f = -\frac{1}{4\pi}\int \mathbf{D}\cdot d\mathbf{E}, \tag{2.6}$$

where $\mathbf{E}$ is the electric field and $\mathbf{D}$ is the displacement field [3,24]. The electric displacement field takes the following form in the presence of flexoelectricity:

$$\mathbf{D} = \hat{\varepsilon}\mathbf{E} + 4\pi\mathbf{P}_{\rm flex}, \tag{2.7}$$

where

$$\varepsilon_{\alpha\beta} = \varepsilon_\perp\delta_{\alpha\beta} + \varepsilon_a n_\alpha n_\beta, \tag{2.8}$$

$$\mathbf{P}_{\rm flex} = e_1\mathbf{n}\operatorname{div}\mathbf{n} + e_3\operatorname{curl}\mathbf{n}\times\mathbf{n}, \tag{2.9}$$

$\varepsilon_a = \varepsilon_\parallel - \varepsilon_\perp$, $\varepsilon_\parallel$ and $\varepsilon_\perp$ are permittivities along and across with respect to $\mathbf{n}$; e_1 and e_3 are flexoelectric coefficients [3]. Assuming that the field $\mathbf{E}$ is homogeneous in XY plane, $\mathbf{E}(\mathbf{r}) = \mathbf{E}(z)$, we obtain

$$\mathcal{F}_f = -\frac{S_\perp}{8\pi}\int_0^L \mathbf{E}\cdot\hat{\varepsilon}\mathbf{E}\,dz - S_\perp\int_0^L \mathbf{P}_{\rm flex}\cdot\mathbf{E}\,dz. \tag{2.10}$$

As follows from the Maxwell equation $\operatorname{curl}\mathbf{E} = \mathbf{0}$ and boundary conditions $E_{x,y}(0) = E_{x,y}(L) = 0$, the vector $\mathbf{E}$ has only one nonzero component $E_z = E(z)$. Thus,

$$\mathcal{F}_f = -\frac{S_\perp}{8\pi}\int_0^L E^2(z)\mathcal{E}(\theta)dz + S_\perp\bar{e}\int_0^L \sin 2\theta\,\theta' E(z)dz, \tag{2.11}$$

where

$$\mathcal{E}(\theta) = \varepsilon_\perp + \varepsilon_a\cos^2\theta,\quad \bar{e} = (e_1+e_3)/2. \tag{2.12}$$

The z component D_z is independent of z due to identity $\operatorname{div}\mathbf{D}(z) = 0$. Equation (2.7) gives

$$D_z = \mathcal{E}(\theta)E(z) - 4\pi\bar{e}\sin 2\theta\,\theta', \tag{2.13}$$

and so we get

$$E(z) = (D_z + 4\pi\bar{e}\sin 2\theta\,\theta')/\mathcal{E}(\theta). \tag{2.14}$$

The magnitude of D_z and the voltage U applied to the electrodes are related as follows:

$$U = \int_0^L E(z)\,dz = D_z J^{-1} + 4\pi\bar{e}J_1, \tag{2.15}$$

where

$$J^{-1} = \int_0^L \frac{dz}{\mathcal{E}(\theta)}, \quad J_1 = \varepsilon_a^{-1} \ln\frac{\mathcal{E}(\theta(0))}{\mathcal{E}(\theta(L))}. \tag{2.16}$$

It is notable that the factor J_1 depends on $\theta(z)$ only via its values at the boundaries $\theta(0)$ and $\theta(L)$. Thus, we have

$$D_z = (U - 4\pi\bar{e}J_1)J, \tag{2.17}$$

and the electric field takes the form

$$E(z) = [UJ + 4\pi\bar{e}(\sin 2\theta\,\theta' - J_1 J)]/\mathcal{E}(\theta). \tag{2.18}$$

Note that Eq. (2.17) is analogous to Eq. (3) in Ref. [17], though our result differs by a factor $\bar{e}$ instead of sum $e_1 + e_3$.

Substituting Eq. (2.18) into (2.11), we obtain

$$\mathcal{F}_f = -\frac{S_\perp}{8\pi}U^2 J + S_\perp \bar{e} U J J_1 + 2\pi S_\perp \bar{e}^2\left(\int_0^L \frac{(\sin 2\theta\,\theta')^2}{\mathcal{E}(\theta)}dz - J J_1^2\right). \tag{2.19}$$

Here, the spatial inhomogeneity of the electric field induced by flexoelectricity is taken into account. In the case of LC without flexoelectricity, $\bar{e} = 0$, we obtain (cf. Refs. [6,7,12])

$$\mathcal{F}_f = -S_\perp U^2 J/8\pi. \tag{2.20}$$

If $(\varepsilon_a/\varepsilon_\perp)\cos^2\theta \ll 1$, Eq. (2.20) reduces to the simpler form [3]

$$\mathcal{F}_f = \mathcal{F}_f^{(0)} - \frac{S_\perp \varepsilon_a U^2}{8\pi L^2}\int_0^L \cos^2\theta\,dz, \quad \mathcal{F}_f^{(0)} = -\frac{S_\perp U^2 \varepsilon_\perp}{8\pi L},$$

accounting for the inhomogeneity of the director $\mathbf{n}(z)$ and ignoring the inhomogeneity of the electric field.

Note that $\mathcal{F}_f$ depends on the sign of the voltage U due to the flexoelectric term $S_\perp \bar{e} U J J_1$ in Eq. (2.19). In the case of rigid symmetric boundary condition $\theta(0) = \theta(L)$, this term vanishes since $J_1 = 0$. We assume that $\bar{e} > 0$. The case $\bar{e} < 0$ can be reduced to the case $\bar{e} > 0$ by changing $(\bar{e}, U) \to (-\bar{e}, -U)$. It is notable that in accordance to Eq. (2.18) the nonzero electric field appears in flexoelectric inhomogeneous system even if $U = 0$. This electric field induced by the director distortion gives rise to the last term in Eq. (2.19).

It is noteworthy that the last term of Eq. (2.19) describing the contribution of the electric field to the free energy can be rewritten as

$$2\pi S_\perp \bar{e}^2 \int_0^L \frac{(\sin 2\theta\,\theta' - J J_1)^2}{\mathcal{E}(\theta)}dz. \tag{2.21}$$

Hence, for large $\bar{e}$ and for not too high voltages U the electric field contribution takes the minimum value if $\sin 2\theta\,\theta' - J J_1 = 0$. This functional integrodifferential equation can be solved in an explicit form. Its general solution can be presented as

$$\cos^2\theta(z) = az + b \tag{2.22}$$

with both constants a and b being surprisingly arbitrary. This formula defines the $\theta(z)$ profile form for sufficiently high $\bar{e}$.

Collecting the elastic, anchoring, and electric field terms we obtain the ultimate total distortion free energy

$$\mathcal{F}_{\rm tot} = \mathcal{F}_e^{(0)} + \frac{S_\perp}{2}\int_0^L [\mathcal{A}(\theta)(\theta')^2 + B(\theta)(\varphi')^2 - 2C(\theta)\varphi']dz + \frac{S_\perp}{2}\sum_{\alpha=1,2}\left[W_\theta^{(\alpha)}\sin^2\left(\theta - \theta_0^{(\alpha)}\right) + W_\varphi^{(\alpha)}\sin^2\left(\varphi - \varphi_0^{(\alpha)}\right)\right] - S_\perp \mathcal{U}^2 J/8\pi, \tag{2.23}$$

where

$$\mathcal{A}(\theta) = A(\theta) + 4\pi\bar{e}^2\sin^2 2\theta/\mathcal{E}(\theta), \ \mathcal{U} = U - 4\pi\bar{e}J_1 \tag{2.24}$$

can be treated as functions renormalized by flexoelectricity.

III. EQUILIBRIUM STRUCTURE

A. Euler-Lagrange equations and elimination of azimuthal angle

The first variation of the distortion free energy can be presented as

$$\delta\mathcal{F}_{\rm tot} = S_\perp\left\{\int_0^L\left[\frac{1}{2}\frac{d\mathcal{A}}{d\theta}\theta'^2\delta\theta + \mathcal{A}\theta'(\delta\theta)' + \frac{1}{2}\frac{dB}{d\theta}\varphi'^2\delta\theta + B\varphi'(\delta\varphi)' - \frac{dC}{d\theta}\varphi'\delta\theta - C(\delta\varphi)'\right]dz + \frac{1}{2}\sum_{\alpha=1,2}\left[W_\theta^{(\alpha)}\sin 2\left(\theta_\alpha - \theta_0^{(\alpha)}\right)\delta\theta_\alpha + W_\varphi^{(\alpha)}\sin 2\left(\varphi_\alpha - \varphi_0^{(\alpha)}\right)\delta\varphi_\alpha\right] + \frac{\varepsilon_a}{8\pi}\mathcal{U}^2 J^2\int_0^L \frac{\sin 2\theta}{\mathcal{E}^2(\theta)}\delta\theta\,dz + \bar{e}\mathcal{U}J\frac{\sin 2\theta}{\mathcal{E}(\theta)}\delta\theta\Big|_0^L\right\},$$

where $\theta_\alpha = \theta(l_\alpha)$, $\varphi_\alpha = \varphi(l_\alpha)$, and $l_1 = 0$, $l_2 = L$. Equating $\delta\mathcal{F}_{\rm tot}$ to zero for arbitrary variations $\delta\theta$ and $\delta\varphi$ in the bulk and at the boundaries, we obtain a set of two Euler-Lagrange equations and two boundary conditions. Integrating by parts the elastic term in $\delta\mathcal{F}_{\rm tot}$, we get the equation set

$$\frac{d\mathcal{A}}{d\theta}\theta'^2 + 2\mathcal{A}\theta'' = \frac{dB}{d\theta}\varphi'^2 - 2\frac{dC}{d\theta}\varphi' + \frac{\varepsilon_a \mathcal{U}^2 J^2\sin 2\theta}{4\pi\mathcal{E}^2(\theta)}, \tag{3.1}$$

$$d(B\varphi' - C)/dz = 0, \tag{3.2}$$

with the boundary conditions

$$\left(2(-1)^\alpha[\mathcal{A}(\theta)\theta' + \bar{e}\mathcal{U}J\sin 2\theta/\mathcal{E}(\theta)] + W_\theta^{(\alpha)}\sin 2\left(\theta - \theta_0^{(\alpha)}\right)\right)\Big|_{z=l_\alpha} = 0, \tag{3.3}$$

$$\left(2(-1)^\alpha(B\varphi' - C) + W_\varphi^{(\alpha)}\sin 2\left(\varphi - \varphi_0^{(\alpha)}\right)\right)\Big|_{z=l_\alpha} = 0, \tag{3.4}$$

where $\alpha = 1, 2$. Note that Eq. (3.1) is the functional integrodifferential equation since the factor J_1 contains values $\theta(0)$ and $\theta(L)$ and the factor J depends on the function $\theta(z)$ within the bulk. It should be noted as well that Eqs. (3.3) are integral nonlocal boundary conditions. These features have arisen due to the flexoelectricity. The first integral of equation set (3.1) and (3.2) is given by

$$\mathcal{A}(\theta)\theta'^2 + B(\theta)\varphi'^2 - \mathcal{U}^2 J^2/(4\pi\mathcal{E}(\theta)) = C_1, \quad (3.5)$$

$$B(\theta)\varphi' - C(\theta) = C_2, \quad (3.6)$$

where $C_{1,2}$ are arbitrary constants. The particular integrals can be found from the boundary conditions (3.3) and (3.4).

We are going to find the LC equilibrium structure by the variational method minimizing the free energy numerically. The equilibrium and boundary conditions (3.6) and (3.4) will be used for the simplification of $\mathcal{F}_{\rm tot}$, and Eqs. (3.5) and (3.3) to control accuracy of the minimization results. Restricting ourselves to the equilibrium distributions of $\theta(z)$ and $\varphi(z)$, we can present $\mathcal{F}_{\rm tot}$ as a functional of the function $\theta(z)$ only.

Substituting Eq. (3.6) into (2.4), we obtain

$$\mathcal{F}_e = \mathcal{F}_e^{(0)} + \frac{S_\perp}{2}\int_0^L \left[A(\theta)\theta'^2 + \frac{C_2^2 - C^2(\theta)}{B(\theta)}\right] dz. \quad (3.7)$$

Integration of Eq. (3.6) over the interval $[0; L]$ gives

$$\varphi_{\rm tot} = C_2 I_1 + I_2, \quad (3.8)$$

where $\varphi_{\rm tot} = \varphi(L) - \varphi(0)$, and

$$I_1 = \int_0^L \frac{dz}{B(\theta)}, \; I_2 = \int_0^L \frac{C(\theta)}{B(\theta)}\, dz.$$

Inserting Eq. (3.6) into (3.4), we get

$$2\big(\varphi(l_\alpha) - \varphi_0^{(\alpha)}\big) = (-1)^{\alpha+1} \arcsin\big(2C_2/W_\varphi^{(\alpha)}\big), \quad (3.9)$$

$\alpha = 1,2$, and hence

$$2\big(\varphi_{\rm tot}^{(0)} - \varphi_{\rm tot}\big) = \arcsin\big(2C_2/W_\varphi^{(1)}\big) + \arcsin\big(2C_2/W_\varphi^{(2)}\big), \quad (3.10)$$

where $\varphi_{\rm tot}^{(0)} = \varphi_0^{(2)} - \varphi_0^{(1)}$. Here, we assume that $|\varphi(l_\alpha) - \varphi_0^{(\alpha)}| \leqslant \pi/4$. It is a regular situation which excludes the effects of jumps in a cholesteric pitch [25].

Equations (3.8) and (3.10) yield the equation for C_2,

$$C_2 = \big(\varphi_{\rm tot}^{(0)} - I_2\big)\big/\big(I_1 + k_1/W_\varphi^{(1)} + k_2/W_\varphi^{(2)}\big), \quad (3.11)$$

where $k_\alpha = (W_\varphi^{(\alpha)}/2C_2)\arcsin(2C_2/W_\varphi^{(\alpha)})$, $1 \leqslant k_\alpha \leqslant \pi/2$. The inequalities $|C_2|/W_\varphi^{(\alpha)} \leqslant 0.5$ must be valid for the solution of Eq. (3.11). For $|C_2|/W_\varphi^{(\alpha)} \ll 1$ we get the explicit formula

$$C_2 = (\varphi_{\rm tot}^{(0)} - I_2)\big(I_1 + 2/W_\varphi^H\big)^{-1} \quad (3.12)$$

with $W_\varphi^H = 2W_\varphi^{(1)}W_\varphi^{(2)}/(W_\varphi^{(1)} + W_\varphi^{(2)})$.

Substituting Eq. (3.11) into (3.7) and using Eq. (3.9) we find $\mathcal{F}_{\rm tot}$ as a functional of $\theta(z)$:

$$\mathcal{F}_{\rm tot}(\theta) = \mathcal{F}_e^{(0)} + \frac{S_\perp}{2}\Bigg[\int_0^L \left(\mathcal{A}(\theta)\theta'^2 - \frac{C^2(\theta)}{B(\theta)}\right)dz + W_\theta^{(1)}\sin^2\big(\theta(0) - \theta_0^{(1)}\big) + W_\theta^{(2)}\sin^2\big(\theta(L) - \theta_0^{(2)}\big) + C_2^2\big(I_1 + \kappa_1/W_\varphi^{(1)} + \kappa_2/W_\varphi^{(2)}\big) - \frac{\mathcal{U}^2 J}{4\pi}\Bigg], \quad (3.13)$$

where $\kappa_\alpha = 2/(1 + \sqrt{1 - (2C_2/W_\varphi^{(\alpha)})^2})$, $1 \leqslant \kappa_\alpha \leqslant 2$. The next-to-last term in $\mathcal{F}_{\rm tot}(\theta)$ for $|C_2|/W_\varphi^{(\alpha)} \ll 1$ takes the explicit form

$$\frac{S_\perp}{2}\big(\varphi_{\rm tot}^{(0)} - I_2\big)^2\big(I_1 + 2/W_\varphi^H\big)^{-1}. \quad (3.14)$$

The error of this approximation is about 2% for $|C_2|/W_\varphi^{(\alpha)} \leqslant 0.25$ and about 15% for the whole area $|C_2|/W_\varphi^{(\alpha)} \leqslant 1/2$.

Assuming the equilibrium function $\theta(z)$ being determined one can find the equilibrium function $\varphi(z)$ from Eqs. (3.6), (3.4), and (3.11):

$$\varphi(z) = \varphi_0^{(1)} + \frac{1}{2}\arcsin\frac{2C_2}{W_\varphi^{(1)}} + \int_0^z \frac{C(\theta) + C_2}{B(\theta)}\, dz. \quad (3.15)$$

B. Numerical analysis

Equilibrium orientational structure in the LC cell is obtained by a numerical minimization of the free energy (3.13) using the following easy directions at the boundaries:

$$\theta_0^{(1)} = \theta_0^{(2)} = \pi/2, \; \varphi_{\rm tot}^{(0)} = q_0 L. \quad (3.16)$$

These conditions correspond to the unstressed twisted LC in the absence of the electric field. The function $\theta(z)$ is described by the trial function

$$\theta(z) = \pi/2 + \delta\psi(z, \delta_1, \delta_2) + \sum_{n=1}^{N} c_n \sin(\pi n z/L). \quad (3.17)$$

Here, the term $\pi/2$ corresponds to the undistorted state. The function $\delta\psi(z, \delta_1, \delta_2)$, given by Eq. (4.12), arises from the orientational distortions at the boundaries: $\theta(0) = \pi/2 + \delta_1$, $\theta(L) = \pi/2 + \delta_2$. The Fourier sum describes bulk distortions of the director. Fourier coefficients c_N and c_{N-1} can be obtained explicitly as functions of $\delta_{1,2}$ and $\{c_n\}_{n=1}^{N-2}$ using boundary conditions (3.3). Thus, the angles δ_1, δ_2, and the coefficients c_n, $n = 1, \ldots, N-2$, are adjustable parameters.

We restrict ourselves to $N = 20$ in the Fourier series (3.17). Accounting for more than 20 terms would change the relative deviation of θ less than by 0.5% for all z. In multidimensional numerical minimization there exists the problem of being trapped by saddle points or maxima. We use small random shifts of obtained parameters $\delta_{1,2}$, $\{c_n\}$ to distinguish real minima. If the minimization algorithm leads to a different point, we have a saddle point or a maximum. For minima, the minimization always returns back.

Let us change the voltage U, keeping other LC cell parameters fixed. Three cases are found:

(a) The single minimum case corresponds to the planar helicoidal structure, where $\delta_{1,2} = 0$ and $c_n = 0$, i.e., $\theta(z) = \pi/2$, and $\varphi(z) = q_0 z$.

(b) The three minima case. The first of them corresponds again to the planar helicoidal "phase." Two extra minima M_1 and M_2 correspond to the distorted "phases," where some of the parameters $\delta_{1,2}$, c_n are nonzero. The points M_1 and M_2 are transferred into each other by the substitution $(\delta_1, \delta_2, c_n) \rightarrow$

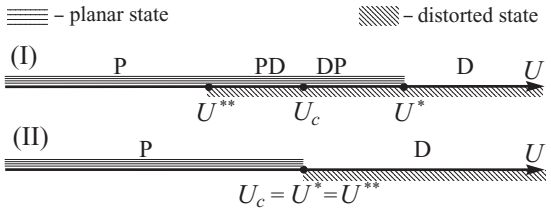

FIG. 1. A sketch illustrating discontinuous (I) and continuous (II) Fréedericksz transitions for $U > 0$. (I) The stability areas for the distorted (D) "phase" $U > U^{**}$, and for the undistorted planar (P) "phase" $U < U^{*}$. In the interval PD, $U^{**} < U < U_c$, the D phase is metastable, and in the interval DP, $U_c < U < U^{*}$, the P phase is metastable. (II) The stability intervals for the distorted "phase" $U > U_c$, and for the undistorted planar "phase" $U < U_c$.

$(-\delta_1, -\delta_2, -c_n)$. The states M_1 and M_2 correspond to the same director distribution due to the symmetry $\mathbf{n} \leftrightarrow -\mathbf{n}$.

(c) Two minima M_1 and M_2 correspond to the distorted "phases." The planar helicoidal "phase" does not exist in this case.

1. Phase diagram

The case (a) occurs for voltages $|U|$ below the threshold value U^{**}. Two possible situations can be observed when the voltage exceeds U^{**}. They correspond to the discontinuous (I) and continuous (II) Fréedericksz transition:

I. There exists one more threshold $U^{*} > U^{**}$ producing the case (b) for $|U| \in (U^{**}, U^{*})$. Here, U^{**} is the lowest voltage at which the distorted "phase" can exist as a metastable state, and, in its turn, U^{*} is the highest voltage at which the planar helicoidal "phase" can exist as a metastable state. In the interval (U^{**}, U^{*}) one of the "phases" can exist as a metastable one. The system energy in the distorted "phase" decreases with the increase of the voltage $|U|$. Eventually, the energies of the system in the distorted and in the planar "phases" become equal at some voltage $|U| = U_c$, and the discontinuous Fréedericksz transition takes place. For $|U| < U_c$ the system is in the undistorted state, and for $|U| > U_c$ it is in the distorted state. Finally, for $|U| > U^{*}$ we have case (c).

II. There exists only one threshold voltage $|U| = U_c$. This case corresponds to situation I with $U^{*} = U_c = U^{**}$ and the Fréedericksz transition is continuous. For $|U| < U_c$ we have case (a) and for $|U| > U_c$ – case (c).

The stability and metastability voltage intervals are presented in Fig. 1. Here and elsewhere, we use the term "stable" for equilibrium states corresponding to local minima of the free energy. The term "metastable" is used for a stable state with the free energy exceeding that of another stable state.

In order to examine the flexoelectricity effect on the Fréedericksz transition, we calculated the voltages U^{**}, U_c, U^{*} depending on $\bar{e}$. Note that the account for the flexoelectricity makes the values U^{**}, U^{*}, and U_c different for $U > 0$ and for $U < 0$ if $W_\theta^{(1)} \neq W_\theta^{(2)}$. The material constants were taken the same as in Ref. [12]: $K_{11} = 0.42 \times 10^{-6}$ dyn, $K_{22} = 0.23 \times 10^{-6}$ dyn, $K_{33} = 0.53 \times 10^{-6}$ dyn, $q_0 = 500$ cm^{-1}, $L = 60$ μm, $W_\theta^{(1)} = 2.5 \times 10^{-3}$ erg/cm^2, $W_\theta^{(2)} = 0.5 \times 10^{-3}$ erg/cm^2, $W_\varphi^{(1)} = 2.5 \times 10^{-4}$ erg/cm^2, $W_\varphi^{(2)} = 1.0 \times 10^{-4}$ erg/cm^2, $\varepsilon_\perp = 7.2$, $\varepsilon_\parallel = 16.2$. The

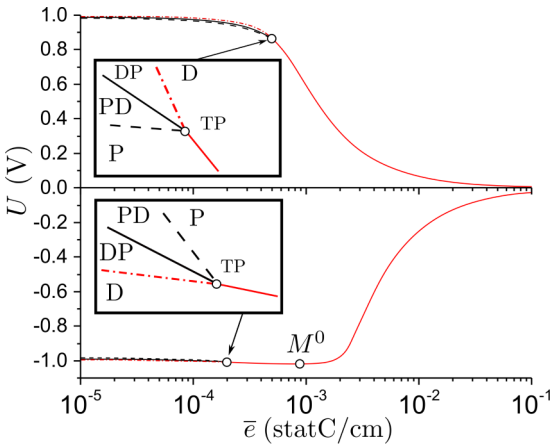

FIG. 2. Phase diagram. The voltages U^{*}, U_c, and U^{**} as functions of the mean flexoelectric coefficient $\bar{e}$: dashed line, U^{**}; solid line, U_c; dashed-dotted line, U^{*}. The stability and metastability areas are schematically shown in the insets. The tricritical points are denoted by TP, other notations are the same as in Fig. 1. The lines U^{*}, U_c, and U^{**} coincide to the right of TPs.

parameters q_0 and L correspond to the supertwisted LC cell with $q_0 L = 3 > \pi/2$. We have chosen sufficiently different anchoring constants in order to demonstrate the influence of the boundary asymmetry. In Fig. 2 we present the calculated phase diagram in the $(\bar{e}, U)$ plane for both directions of the electric field. It is noteworthy that in the case of $U > 0$ the voltages U^{*}, U_c, and U^{**} decrease with the increase of $\bar{e}$, thus, flexoelectricity promotes the transition. However, the dependencies of voltages on $\bar{e}$ are nonmonotonic for $U < 0$ (the minimum point is denoted by M^0). In the case of symmetric boundary conditions, $W_\theta^{(1)} = W_\theta^{(2)}$ and $W_\varphi^{(1)} = W_\varphi^{(2)}$, the curves U^{*}, U_c, and U^{**} are symmetric with respect to the $\bar{e}$ axis. The Fréedericksz transition turns out to be discontinuous at lower $\bar{e}$ and continuous at higher $\bar{e}$. Such a change of the transition type occurs in the tricritical point TP. The vicinity of the tricritical point is shown schematically in the inset of Fig. 2.

2. Equilibrium state

Equilibrium $\theta(z)$ and $\varphi(z)$ profiles are presented in Fig. 3 with the same material parameters as in Fig. 2 for different values of $\bar{e}$. It is interesting to point out to several specific features of these plots. First, the shape of the curves $\theta(z)$ and $\varphi(z)$ changes considerably as $\bar{e}$ rises. The dependence $\theta(z)$ is described by a simple formula (2.22) for sufficiently high values of $\bar{e}$. Second, the asymmetry of $\theta(z)$ profile with the respect of the center $z = L/2$ increases significantly for high $\bar{e}$; in particular, $\theta(0) \to \pi/2$ and $\theta(L) \to 0$ if $\bar{e} \to \infty$. Here, we have the planar → hybrid aligned Fréedericksz transition for a system with strong flexoelectricity instead of planar → homeotropic one for a system without flexoelectricity.

It is important to note that due to flexoelectricity the $\theta(z)$ profiles remain asymmetric even in systems with the same anchoring modules at both boundaries. This phenomenon is illustrated in Fig. 4: it is notable that if $U > 0$, then $\theta(0) \approx \pi/2$ and $\theta(L) \approx 0$ for large $\bar{e}$. It can be explained as follows: the profile $\theta(z)$ obeys Eq. (2.22) for high $\bar{e}$, and so the last

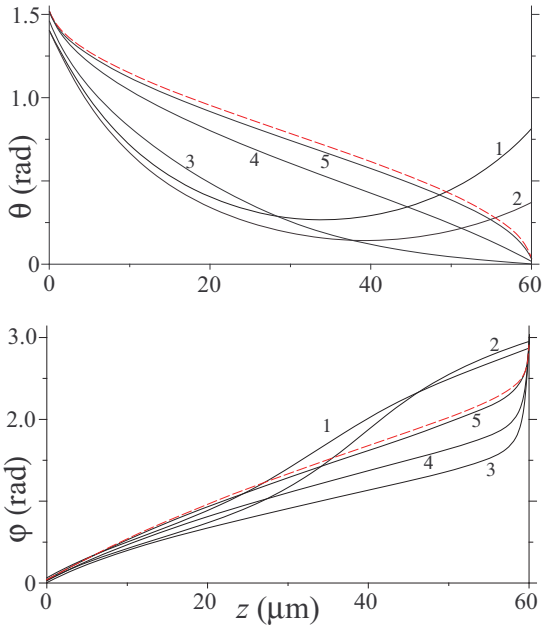

FIG. 3. Equilibrium profiles $\theta(z)$ and $\varphi(z)$ calculated via Eq. (3.17) for $U = 1.2$ V. Lines 1 correspond to the LC without flexoelectricity, $\bar{e} = 0$; lines 2 are for $\bar{e} = 10^{-4}$ statC/cm, lines 3 are for $\bar{e} = 10^{-3}$ statC/cm, lines 4 are for $\bar{e} = 3 \times 10^{-3}$ statC/cm, and lines 5 are for $\bar{e} = 10^{-2}$ statC/cm (we use the statcoulomb unit, statC, for electric charge in cgs system). Dashed lines (red online) are calculated via formulas (3.18) and (3.19).

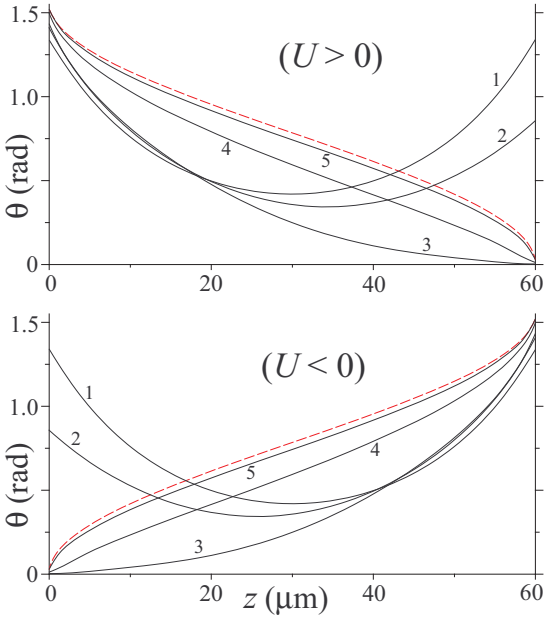

FIG. 4. Equilibrium profiles $\theta(z)$ for $U = \pm 1.2$ V in the case of symmetric anchoring: $W_\theta^{(1)} = W_\theta^{(2)} = 1.5 \times 10^{-3}$ erg/cm^2 and $W_\varphi^{(1)} = W_\varphi^{(2)} = 1.5 \times 10^{-4}$ erg/cm^2. The lines' numbers, $\bar{e}$ values, and other material parameters are the same as in Fig. 3, except line 2, which corresponds to $\bar{e} = 5 \times 10^{-4}$ statC/cm. Dashed lines (red online) are calculated via formula (3.18).

term in the free energy (2.19) is close to zero. Hence, the main input into $\mathcal{F}_f$ is given by the second term $S_\perp \bar{e} U J J_1 \approx S_\perp \bar{e} U \sin 2\theta\, \theta' = -S_\perp \bar{e} U (\cos^2\theta)' \approx -S_\perp \bar{e} U a$. In order to minimize $\mathcal{F}_f$, one should have the maximal value of $a\,\mathrm{sgn}(\bar{e}U)$. Note that $aL = \cos^2\theta(L) - \cos^2\theta(0)$. So, the minimum of $\mathcal{F}_f$ is attained when $\theta(0) \approx \pi/2, \theta(L) \approx 0$ for $\bar{e}U > 0$ and $\theta(0) \approx 0$, $\theta(L) \approx \pi/2$ for $\bar{e}U < 0$. Hence, according to Eqs. (2.22) and (3.15), the profiles for large $\bar{e}$ have the form

$$\theta(z) \simeq \begin{cases} \arccos\sqrt{z/L}, & \bar{e}U > 0 \\ \arccos\sqrt{1 - z/L}, & \bar{e}U < 0 \end{cases} \tag{3.18}$$

$$\varphi(z) \simeq \begin{cases} \varphi_0^{(1)} + \frac{q_0 L}{\zeta} \ln\left(1 + \zeta \frac{z}{L}\right), & \bar{e}U > 0 \\ \varphi_0^{(2)} - \frac{q_0 L}{\zeta} \ln\left[1 + \zeta\left(1 - \frac{z}{L}\right)\right], & \bar{e}U < 0 \end{cases} \tag{3.19}$$

where $\zeta = (K_{33} - K_{22})/K_{22}$. Note that the first formula in (3.19) is invalid in the vicinity of $z = L$, and the second one is invalid in the vicinity of $z = 0$. In order to describe the dependence $\varphi(z)$ near these points, it is necessary to take into account the small corrections $\sim 1/\bar{e}$ in Eq. (3.18).

Now, let us discuss how the continuity and discontinuity of the Frèedericksz transition affects the director orientation structure just above the threshold. It can be seen from Fig. 2 that the region of the phase coexistence is very narrow for the material parameters given. In such a situation it seems reasonable to expect that discontinuity of the transition does not manifest itself in the director structure notably. For checking purposes, we calculated the profiles for two different values of $\bar{e}$, i.e., below and above $\bar{e}^{\mathrm{TP}}$ at the different voltages applied. If the voltage is below U_c, the system remains in the planar helicoidal state, after that the structure at the voltage above U_c by 0.5% was explored. It was found that there is a significant difference between $\theta(z)$ profiles for the cases of continuous and discontinuous transitions (Fig. 5). Consequently, the discontinuity of the transition radically changes the director structure above the threshold even if there is only a very small difference between U^* and U^{**}.

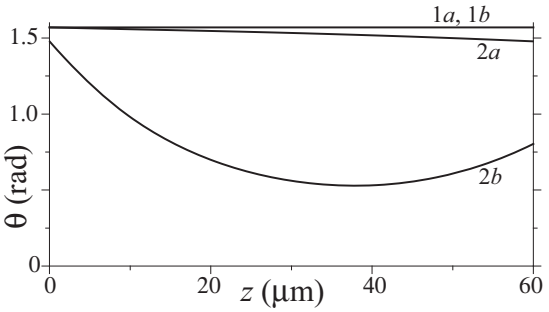

FIG. 5. Profiles $\theta(z)$ for continuous (a) and discontinuous (b) transitions. Coinciding lines 1a and 1b refer to the planar helicoidal structure ($U = 0.999U_c$) and lines with the number 2 correspond to the distorted structures ($U = 1.005U_c$). For "a" profiles $\bar{e} = 8 \times 10^{-4}$ statC/cm $> \bar{e}^{\mathrm{TP}}$ and for "b" profiles $\bar{e} = 2 \times 10^{-4}$ statC/cm $< \bar{e}^{\mathrm{TP}}$, where $\bar{e}^{\mathrm{TP}} = 5.132 \times 10^{-4}$ statC/cm. The threshold voltages are (a) $U_c = 0.6926$ V, (b) $U_c = 0.9396$ V. Other material parameters are the same as in Fig. 3.

IV. STABILITY OF THE PLANAR HELICOIDAL STRUCTURE. ANALYTICAL APPROACH

The pair of angle functions $\theta_0(z) = \pi/2$, $\varphi_0(z) = q_0 z$ with $z \in [0,\ L]$ describes the undistorted planar helicoidal structure. Investigating its stability we are to study the second variation of the free energy $\mathcal{F}_{\rm tot}(\theta_0, \varphi_0)$. It has already been obtained in Ref. [12] when flexoelectricity is absent:

$$\delta^2\mathcal{F}_{\rm tot}|_{\bar e=0} = \frac{S_\perp}{2}\Big[\int_0^L (K_{11}(\delta\theta')^2 + M\delta\theta^2 + K_{22}(\delta\varphi')^2)\,dz + \sum_{\alpha=1,2} W_\theta^{(\alpha)}\delta\theta^2(l_\alpha) + \sum_{\alpha=1,2} W_\varphi^{(\alpha)}\delta\varphi^2(l_\alpha)\Big], \tag{4.1}$$

where

$$M = K_{33}q_0^2 - \varepsilon_a U^2/(4\pi L^2). \tag{4.2}$$

As long as $J_1|_{\theta=\theta_0} = 0$ and $\delta J_1|_{\theta=\theta_0} = 0$, the flexoelectricity contribution to the second variation of $\mathcal{F}_{\rm tot}$ is given by

$$\delta^2\mathcal{F}_{\rm flex} = -S_\perp \bar e (U/L)\delta\theta^2\big|_0^L. \tag{4.3}$$

Hence, $\delta^2\mathcal{F}_{\rm tot} = \delta^2\mathcal{F}_{\rm tot}|_{\bar e=0} + \delta^2\mathcal{F}_{\rm flex}$ turns to be a sum of two independent variations corresponded to the angles θ and φ. The part depending on φ is positive definite due to inequalities $K_{22} > 0$ and $W_\varphi^{(1,2)} > 0$. So, the stability of the planar helicoidal structure is determined by the terms depending on θ variation only:

$$\delta^2\mathcal{F}_\theta = \frac{S_\perp}{2}\int_0^L (K_{11}(\delta\theta')^2 + M(\delta\theta)^2)dz + \frac{S_\perp}{2}\sum_{\alpha=1,2}\mathcal{W}^{(\alpha)}\delta\theta^2(l_\alpha), \tag{4.4}$$

where

$$\mathcal{W}^{(\alpha)} = W_\theta^{(\alpha)} - 2(-1)^\alpha \bar e U/L. \tag{4.5}$$

So, the contribution of flexoelectricity to $\delta^2\mathcal{F}_{\rm tot}$ reduces to the renormalization of the surface elastic modules, i.e., $W_\theta^{(\alpha)} \to \mathcal{W}^{(\alpha)}$. It is noteworthy that one of the "effective" anchoring energies $\mathcal{W}^{(\alpha)}$ increases and remains positive, while the second one decreases and becomes negative when the applied voltage $|U|$ is high enough. The following notation will be used further:

$$\mathcal{W}^+ = \begin{cases}\mathcal{W}^{(1)}, & \text{if } U > 0\\ \mathcal{W}^{(2)}, & \text{if } U < 0\end{cases} \quad \mathcal{W}^- = \begin{cases}\mathcal{W}^{(2)}, & \text{if } U > 0\\ \mathcal{W}^{(1)}, & \text{if } U < 0.\end{cases} \tag{4.6}$$

As it follows from Eq. (4.4), the planar helicoidal configuration can become unstable only if at least one of the values $\{M, \mathcal{W}^-\}$ is negative. In what follows, we restrict ourselves to the case of $\varepsilon_a > 0$. It turns out that there are three cases of potential instability:

$$\begin{aligned}&\text{I.}\quad M < 0,\quad \mathcal{W}^- \geqslant 0,\\ &\text{II.}\quad M < 0,\quad \mathcal{W}^- < 0,\\ &\text{III.}\quad M \geqslant 0,\quad \mathcal{W}^- < 0.\end{aligned} \tag{4.7}$$

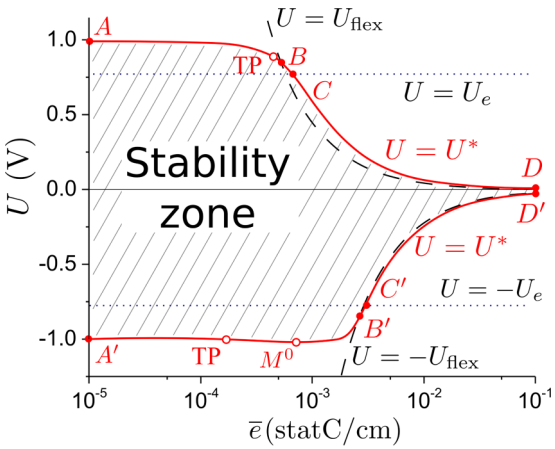

FIG. 6. The curves $ABCD$ and $A'B'C'D'$ plotted using formulas (4.21) present the boundary of the stability zone of the planar helicoidal configuration.

In terms of the voltage U these cases can be rewritten as

$$\begin{aligned}&\text{I.}\quad U_e < |U| \leqslant U_{\rm flex},\\ &\text{II.}\quad |U| > \max(U_e, U_{\rm flex}),\\ &\text{III.}\quad U_{\rm flex} < |U| \leqslant U_e.\end{aligned} \tag{4.8}$$

The areas corresponding to these cases can be seen below in Fig. 6. Here, we used the notations

$$U_e = 2q_0 L\sqrt{\frac{\pi K_{33}}{\varepsilon_a}},\quad U_{\rm flex} = \frac{L}{2\bar e}\begin{cases}W_\theta^{(2)}, & \text{if } U > 0\\ W_\theta^{(1)}, & \text{if } U < 0.\end{cases} \tag{4.9}$$

Analyzing $\delta^2\mathcal{F}_\theta$ we separate $\delta\theta(z)$ into two parts:

$$\delta\theta(z) = \delta\psi(z) + \delta\mu(z), \tag{4.10}$$

where $\delta\mu(0) = \delta\mu(L) = 0$. The function $\delta\psi(z) = \delta\psi(z, \delta_1, \delta_2)$ is chosen in such a way that the following equation and the boundary conditions are satisfied:

$$\begin{aligned}&K_{11}\delta\psi''(z) - M\delta\psi(z) = 0,\\ &\delta\psi(0) = \delta_1,\quad \delta\psi(L) = \delta_2.\end{aligned} \tag{4.11}$$

The solution of Eq. (4.11) can be represented as

$$\delta\psi = \begin{cases}\delta_1\frac{\sin\xi(L-z)}{\sin\xi L} + \delta_2\frac{\sin\xi z}{\sin\xi L}, & M < 0\\ \delta_1(L-z)/L + \delta_2 z/L, & M = 0\\ \delta_1\frac{\sinh\xi(L-z)}{\sinh\xi L} + \delta_2\frac{\sinh\xi z}{\sinh\xi L}, & M > 0\end{cases} \tag{4.12}$$

where the inverse length ξ is defined as

$$\xi = \sqrt{|M|K_{11}^{-1}} = \sqrt{\left|K_{33}q_0^2 - \varepsilon_a U^2/(4\pi L^2)\right|K_{11}^{-1}}. \tag{4.13}$$

Separating $\delta\theta$ into two terms given by Eqs. (4.10) and (4.12), we present $\delta^2\mathcal{F}_\theta$ as a sum of two independent quadratic forms

$$\delta^2\mathcal{F}_\theta = \tfrac{1}{2}S_\perp(Q_\psi + Q_\mu), \tag{4.14}$$

where

$$Q_\psi = \int_0^L (K_{11}\delta\psi'^2(z) + M\delta\psi^2(z))dz + \sum_{\alpha=1,2} \mathcal{W}^{(\alpha)}\delta_\alpha^2, \tag{4.15}$$

$$Q_\mu = \int_0^L (K_{11}(\delta\mu')^2 + M(\delta\mu)^2)dz. \tag{4.16}$$

It is noteworthy that only Q_ψ depends on the boundary distortions $\delta_{1,2}$. Such an approach dates back to Feynman [26] and was used in Refs. [12,27,28] for liquid crystals in bounded cells. Since $K_{11} > 0$, the quadratic form Q_μ is obviously positive definite in the case of $M \geqslant 0$ ($|U| \leqslant U_e$). For $M < 0$ ($|U| > U_e$), the positivity condition of Q_μ is given by [12]

$$\xi L < \pi. \tag{4.17}$$

Substituting Eq. (4.12) into (4.15) we obtain

$$Q_\psi = \begin{cases} \sum_{\alpha=1,2} (K_{11}\xi\cot\xi L + \mathcal{W}^{(\alpha)})\delta_\alpha^2 \\ \qquad - 2K_{11}(\xi/\sin\xi L)\delta_1\delta_2, & \text{if } M < 0 \\ \sum_{\alpha=1,2} (K_{11}/L + \mathcal{W}^{(\alpha)})\delta_\alpha^2 \\ \qquad - 2(K_{11}/L)\delta_1\delta_2, & \text{if } M = 0 \\ \sum_{\alpha=1,2} (K_{11}\xi\coth\xi L + \mathcal{W}^{(\alpha)})\delta_\alpha^2 \\ \qquad -2K_{11}(\xi/\sinh\xi L)\delta_1\delta_2, & \text{if } M > 0. \end{cases} \tag{4.18}$$

Using the Sylvester criterion for the quadratic form Q_ψ and accounting for the inequality (4.17), we obtain the stability conditions for the planar helicoidal structure of a chiral nematic:

$$\text{for } |U| > U_e: \quad \begin{cases} 0 < t < \pi, \\ w^+ + t\cot t > 0, \\ w^{(1)}w^{(2)} + 2\bar{w}t\cot t > t^2, \end{cases} \tag{4.19a}$$

$$\text{for } |U| = U_e: \quad \begin{cases} t = 0, \\ w^+ + 1 > 0, \\ w^{(1)}w^{(2)} + 2\bar{w} > 0, \end{cases} \tag{4.19b}$$

$$\text{for } |U| < U_e: \quad \begin{cases} t > 0, \\ w^+ + t\coth t > 0, \\ w^{(1)}w^{(2)} + 2\bar{w}t\coth t > -t^2, \end{cases} \tag{4.19c}$$

where $t = \xi L$, $w^+ = \mathcal{W}^+ L/K_{11}$, $w^{(\alpha)} = \mathcal{W}^{(\alpha)}L/K_{11}$, and $\bar{w} = (W_\theta^{(1)} + W_\theta^{(2)})L/2K_{11}$ are dimensionless positive parameters. The last inequality in each of the inequalities (4.19) produces the ultimate stability criterion:

$$\begin{aligned} &w^{(1)}w^{(2)} + 2\bar{w}t\cot t - t^2 > 0, && \text{if } |U| > U_e \\ &w^{(1)}w^{(2)} + 2\bar{w} > 0, && \text{if } |U| = U_e \\ &w^{(1)}w^{(2)} + 2\bar{w}t\coth t + t^2 > 0, && \text{if } |U| < U_e. \end{aligned} \tag{4.20}$$

Inequalities (4.20) are transcendental in U. However they are simply quadratic with respect to $\bar{e}$. Hence, the stability conditions can be written explicitly

$$0 \leqslant \bar{e} \leqslant +\infty, \quad \text{if } U = 0 \tag{4.21a}$$

$$0 \leqslant \bar{e} < e_+^*, \quad \text{if } 0 < |U| < U_1 \tag{4.21b}$$

$$e_-^* < \bar{e} < e_+^*, \quad \text{if } U_1 \leqslant |U| < U_2,\ U\Delta w > 0 \tag{4.21c}$$

$$\bar{e} \in \varnothing, \quad \text{if } U_1 \leqslant |U| < U_2,\ U\Delta w < 0 \tag{4.21d}$$

$$\bar{e} \in \varnothing, \quad \text{if } |U| \geqslant U_2 \tag{4.21e}$$

where $\Delta w = (W_\theta^{(2)} - W_\theta^{(1)})L/K_{11}$,

$$e_\pm^*(U) = (K_{11}/4U)(\Delta w \pm 2\bar{w}\,\mathrm{sgn}\,U\sqrt{1 + X(U)}), \tag{4.22}$$

$$X(U) = \frac{2}{\bar{w}} \times \begin{cases} t\cot t - t^2/2\bar{w}, & \text{if } |U| > U_e \\ 1, & \text{if } |U| = U_e \\ t\coth t + t^2/2\bar{w}, & \text{if } |U| < U_e \end{cases} \tag{4.23}$$

and

$$U_i = \sqrt{4\pi K_{11}\varepsilon_a^{-1}t_i^2 + U_e^2},$$

$i = 1, 2$. Here, $t_1, t_2 \in (0; \pi)$ are the roots of the two equations

$$2t\cot t - t^2/\bar{w} = -w_H, \quad t\tan(t/2) = \bar{w} \tag{4.24}$$

correspondingly, where

$$w_H = \frac{2W_\theta^{(1)}W_\theta^{(2)}}{W_\theta^{(1)} + W_\theta^{(2)}}\frac{L}{K_{11}}.$$

The first of Eqs. (4.24) follows from the requirement $e_+^* = 0$ or $e_-^* = 0$, while the second one is caused by the condition $1 + X(U) = 0$. Note that in the case of symmetric boundary conditions, the voltages U_1 and U_2 occur equal, and Eqs. (4.21c) and (4.21d) are eliminated.

The asymptotics of t_1 takes the form

$$t_1 \sim \begin{cases} \pi\left[1 + \frac{2}{w_H} - \pi^2\left(\frac{8}{3w_H^3} - \frac{2}{\bar{w}w_H^2}\right)\right]^{-1}, & w_H \gg 1 \\ \frac{\pi}{2} + \frac{w_H}{\pi} - \frac{\pi}{4\bar{w}} - \frac{2w_H^2}{\pi^3} + \frac{\pi}{8\bar{w}^2}, & w_H \ll 1 \ll \bar{w} \\ \left(\frac{1}{2\bar{w}} + \frac{1}{3} - \frac{w_H}{4\bar{w}} + \frac{2\bar{w}}{45} - \frac{w_H}{6} + \frac{w_H^2}{8\bar{w}}\right)^{-1/2}, & \bar{w} \ll 1. \end{cases}$$

Quite a good approximation for t_2 is [12]

$$t_2 \cong \begin{cases} \pi(1 + 2\bar{w}^{-1} - 2.5\bar{w}^{-3})^{-1}, & \bar{w} \geqslant 3.3 \\ (0.5\bar{w}^{-1} + 0.088)^{-1/2}, & \bar{w} < 3.3. \end{cases}$$

Accuracy of this formula is higher than 0.5% for all $\bar{w}$.

In Fig. 6 the stability zone of the planar helicoidal configuration in $(\bar{e}, U)$ plane is plotted using formulas (4.21) with the same material constants as in Fig. 2. The stability zone is localized between the curves $ABCD$ and $A'B'C'D'$, representing the dependence $U = U^*(\bar{e})$. The areas above the curve $ABCD$ and below the curve $A'B'C'D'$ define the instability zone for the planar configuration. Note that the lines U^* in Fig. 2 obtained by the numerical minimization of the free energy are in excellent agreement with the lines U^* in Fig. 6 calculated by the analytical evaluation. The AC and $A'C'$ segments describe the case when the inequality in the first line of Eq. (4.20) turns to the equality, and CD and $C'D'$ segments correspond to the equality in the third line. The physical sense of different parts of the curves $ABCD$

and $A'B'C'D'$ can be explained as follows. At AB and $A'B'$ segments, the bulk distortions are energetically favorable and the two surface distortions are unfavorable both. At CD and $C'D'$ segments, the surface distortions at one of the boundaries are energetically favorable, while the bulk distortions and the surface distortions at another boundary are unfavorable. At BC and $B'C'$ segments, the bulk distortions and the surface distortions on one of the boundaries are energetically favorable. The surface distortions at another boundary are unfavorable. Note that there is a minimum M^0 in the curve $A'B'C'D'$ marked as an open circle. The existence of the extremum in one of the curves $ABCD$ or $A'B'C'D'$ is the common property for the nonsymmetrical case $W_\theta^{(1)} \neq W_\theta^{(2)}$ (minimum in $A'B'C'D'$ for $W_\theta^{(1)} > W_\theta^{(2)}$ and maximum in $ABCD$ for $W_\theta^{(1)} < W_\theta^{(2)}$). The location of the extremum $M^0(\bar{e}^\circ, U^\circ)$ is given by

$$\bar{e}^\circ = \left|W_\theta^{(2)} - W_\theta^{(1)}\right| L/4U_2, \;\; U^\circ = U_2 \operatorname{sgn}\left(W_\theta^{(2)} - W_\theta^{(1)}\right).$$

The asymptotics $U^*(\bar{e})$ for $\bar{e} \to \infty$ can be expressed as

$$U^*(\bar{e}) \sim (K_{11}/4\bar{e})(\Delta w + 2\bar{w}\operatorname{sgn}(U)\sqrt{1 + X(0)}), \quad (4.25)$$

where $X(0) = 2(t_0/\bar{w})\coth t_0 + (t_0/\bar{w})^2$, $t_0 = q_0 L (K_{33}/K_{11})^{1/2}$. From Eq. (4.25) for $X(0) \ll 1$ we obtain $U^* \simeq U_{\text{flex}} \operatorname{sgn}(U)$, hence the lines $U^*(\bar{e})$ become close to the dashed lines in Fig. 6.

V. LOWER HARMONIC EXPANSION AND TWO-PARAMETRIC LANDAU MODEL

The analysis of Sec. IV shows that the loss of stability by the planar helicoidal configuration arises from the fluctuation modes $\delta_{1,2}$. It provides a way to develop a simplified theory of the Fréedericksz transition which accounts for the $\delta_{1,2}$ modes only. For this purpose, we present the fluctuating angle $\theta(z)$ in the form

$$\tilde{\theta}(z; \delta_1, \delta_2) = \pi/2 + \delta\psi(z; \delta_1, \delta_2), \quad (5.1)$$

where $\delta\psi$ is given by Eq. (4.12). Substituting $\tilde{\theta}$ into Eq. (3.13) and assuming that $\delta_{1,2} \ll 1$, we obtain a Landau-type expansion of $\mathcal{F}_{\text{tot}}$. Restricting ourselves by the fourth-order terms it yields

$$\begin{aligned}\mathcal{F}_{\text{tot}}(\delta_1, \delta_2) &\approx \mathcal{F}^{(0)} + \mathcal{F}^{(2)} + \mathcal{F}^{(4)} \\ &= \mathcal{F}^{(0)} + \frac{1}{2}\sum_{k=0}^{2} A_k \delta_1^k \delta_2^{2-k} + \frac{1}{4!}\sum_{k=0}^{4} B_k \delta_1^k \delta_2^{4-k},\end{aligned} \quad (5.2)$$

with $\mathcal{F}^{(0)} = \mathcal{F}_f^{(0)}$. The explicit forms of coefficients A_k are given by Eq. (4.18). The coefficients

$$B_k = \partial^4 \mathcal{F}_{\text{tot}}(\delta_1, \delta_2)/\partial^k \delta_1 \partial^{4-k} \delta_2\big|_{\delta_1=\delta_2=0}, \quad (5.3)$$

$k = 0, \ldots, 4$, are rather cumbersome and we do not present them here in detail.

Below, we assume that all the system parameters are fixed except the voltage U and the flexoelectric coefficient $\bar{e}$. At low voltage, the discriminant $A_1^2 - 4A_0A_2 < 0$, so the quadratic form $\mathcal{F}^{(2)}$ is positive definite, and consequently the planar helicoidal structure is stable. As the voltage magnitude rises up with fixed $\bar{e}$, the discriminant of $\mathcal{F}^{(2)}$ vanishes for $U = U^*(\bar{e})$, and as a result the appropriate inequality (4.20) turns to the equality. If the discriminant becomes positive, the planar helicoidal structure turns to be unstable. Along the lines $U = U^*(\bar{e})$ (plotted in Figs. 2 and 6), the term $\mathcal{F}^{(2)}(U, \bar{e})$ vanishes for $\delta_2 = \varkappa_* \delta_1$ with

$$\varkappa_*(\bar{e}) = -A_1(U^*, \bar{e})/2A_0(U^*, \bar{e}).$$

The director fluctuations in the planar helicoidal structure are anomalously strong at $U = U^*$. In this situation, the type of the transition (continuous or discontinuous) is determined by the sign of the fourth-order term $\mathcal{F}^{(4)}$ at $\delta_2 = \varkappa_* \delta_1$. Inserting $U = U^*$ and $\delta_2 = \varkappa_* \delta_1$ into Eq. (5.2), we obtain

$$\begin{aligned}\mathcal{F}_{\text{tot}}(\delta_1, \varkappa_*\delta_1) &\approx \mathcal{F}^{(0)} + \frac{1}{4!}\delta_1^4 \sum_{k=0}^{4} B_k \varkappa_*^k \\ &\equiv \mathcal{F}^{(0)} + \frac{1}{4!}\tilde{B}\delta_1^4.\end{aligned} \quad (5.4)$$

For $\tilde{B} = \tilde{B}(\bar{e}) > 0$, the transition is continuous at the critical voltage $U_c = U^*$. The opposite case $\tilde{B} < 0$ means that the system at $U = U^*$ is already in a distorted state with the free energy less than $\mathcal{F}^{(0)}$. Hence, the transition is discontinuous and occurs at $U = U_c$ with $|U_c| < |U^*|$. Note, that the Landau model for systems with $\tilde{B} < 0$ requires to include the sixth or higher even order terms in the free energy expansion in order that the free energy being positive in the area of large order parameter components [29]. However, the fourth order expansion is sufficient for analyzing the type of the phase transition. Note that a similar one-parametric Landau model in the same LC cell geometry was studied in [12] for the case $\bar{e} = 0$ with symmetric boundary conditions $W_\theta^{(1)} = W_\theta^{(2)}$, and continuous and discontinuous transitions had also been found.

The tricritical point TP $= (\bar{e}^{\text{TP}}, U^{\text{TP}})$ can be obtained from the equations

$$U = U^*(\bar{e}), \quad \tilde{B}(\bar{e}) = 0.$$

Note that $\tilde{B} < 0$ for $\bar{e} < \bar{e}^{\text{TP}}$ and $\tilde{B} > 0$ for $\bar{e} > \bar{e}^{\text{TP}}$. We determine the sign of $\tilde{B}(\bar{e})$ using coefficients B_k derived from Eqs. (5.3), (3.13), and (5.1) numerically. The results are shown in Fig. 7. The tricritical points TP are defined by the change of $\tilde{B}$ sign: $\bar{e}^{\text{TP}} = 5.132 \times 10^{-4}$ statC/cm for $U > 0$, and $\bar{e}^{\text{TP}} = 1.676 \times 10^{-4}$ statC/cm for $U < 0$. These points are shown in Fig. 6, and they are in excellent agreement with those obtained by the numerical minimization of the free energy (see Fig. 2).

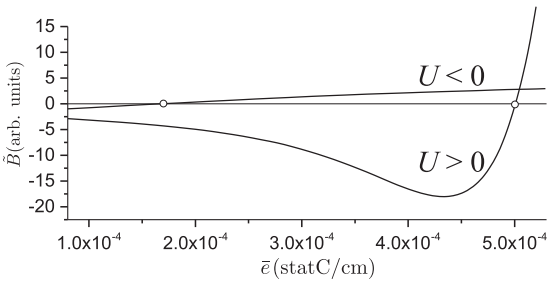

FIG. 7. The effective coefficient $\tilde{B}$ of the Landau model vs the flexoelectric coefficient $\bar{e}$. The material constants are the same as in Figs. 2 and 6. The circles correspond to the tricritical points.

VI. DISCUSSION AND CONCLUSION

In this paper we studied the influence of the flexoelectricity on the Fréedericksz transition in the chiral planar nematic liquid crystal cell with positive dielectric anisotropy. We take into account the inhomogeneity of the external electric field, the flexoelectric effect, and the finite anchoring energy.

Having used the free energy numerical minimization, we obtained the orientational profiles. The stability of equilibrium configurations was investigated numerically. The stability of the planar helicoidal structure was also studied analytically. The dependencies of the threshold voltages U^{**}, U_c, and U^* on the mean flexoelectric coefficient $\bar{e}$ were determined. As a result, the phase diagram in $(\bar{e}, U)$ plane was plotted as well. For the symmetric case $W_\theta^{(1)} = W_\theta^{(2)}$, the Fréedericksz transition voltage U_c was found to decrease monotonously with the coefficient $\bar{e}$ increasing. In the asymmetric case $W_\theta^{(1)} \neq W_\theta^{(2)}$, the dependence of the threshold voltage U_c on the coefficient $\bar{e}$ differs significantly for $U > 0$ and for $U < 0$. In this case, the dependence $U_c(\bar{e})$ is nonmonotonic in one of the two cases, i.e., $U > 0$ or $U < 0$. The phase diagram asymmetry with the respect to the axis $U = 0$ leads to an interesting physical consequence. There exists a voltage interval in which the change of the sign $U \leftrightarrow -U$ results in the change of the LC configuration from the planar helicoidal structure to the distorted one and vice versa ($P \leftrightarrow D$). This effect may be exploited in switching devices. For large mean flexoelectric coefficient $\bar{e}$, the threshold voltage U_c is found to decrease as $1/\bar{e}$. So, the flexoelectricity can be used to reduce the switching voltages in LC devices based on the Fréedericksz transition. It should be noted that the measured data for the flexoelectric coefficients disagree remarkably [13]. Obtained results for the dependence $U_c(\bar{e})$ can be used for a more accurate $e_1 + e_3$ value estimation.

Flexoelectricity gives rise to one more asymmetry type. Namely, the equilibrium profile $\theta(z)$ becomes asymmetric with respect to the center of the LC cell despite the boundary conditions being symmetric. It is interesting to note that for systems with sufficiently high $\bar{e}$ and relatively low U_c, the distorted orientational profile, $\cos^2\theta$, may be approximated by the following linear functions: z/L for $\bar{e}U > 0$ and $1 - z/L$ for $\bar{e}U < 0$. Such profiles exhibit planar orientation at one boundary and homeotropic orientation at another one. It means that as the voltage increases, the LC cell orientational structure changes from the planar helicoidal state to the hybrid-aligned one. This feature may give rise to the development of new flexoelectricity-based switching devices.

Another important issue considered is the type of the Fréedericksz transition, namely, continuous or discontinuous. We studied this problem initially by the numerical minimization of the free energy and thereafter using the Landau-type model with two-parametric order parameter. It was found that the Fréedericksz transition can be either continuous or discontinuous, depending on the cell size and on the LC material parameters. In the phase diagram, the line of continuous phase transitions is separated by the tricritical point from the line of discontinuous phase transition. Note that in the case of discontinuous transition, the phase coexistence region can be very narrow. Despite its narrowness, there is a significant difference between $\theta(z)$ profiles for continuous and discontinuous transitions providing U is above the threshold voltages.

ACKNOWLEDGMENT

The work was supported by the Russian Foundation for Basic Research, Grant No. 16-02-00465a.

[1] D.-K. Yang and S.-T. Wu, *Fundamentals of Liquid Crystal Devices*, 2nd ed., Wiley Series in Display Technology (Wiley, Chichester, 2015).
[2] L. M. Blinov and V. G. Chigrinov, *Electrooptic Effects in Liquid Crystal Materials* (Springer, New York, 1994).
[3] P.-G. de Gennes and J. Prost, *The Physics of Liquid Crystals*, 2nd ed., International Series of Monographs on Physics, Vol. 83 (Clarendon, Oxford, 1993).
[4] I. W. Stewart, *The Static and Dynamic Continuum Theory of Liquid Crystals: A Mathematical Introduction*, Liquid crystals book series (Taylor & Francis, London, 2004).
[5] A. Rapini and M. Papoular, J. Phys. Colloq. **30**, 54 (1969).
[6] H. J. Deuling, Mol. Cryst. Liq. Cryst. **19**, 123 (1972).
[7] H. Gruler, T. J. Scheffer, and G. Meier, Z. Naturforsch. **27a**, 966 (1972).
[8] J. Cheng, R. N. Thurston, and D. W. Berreman, J. Appl. Phys. **52**, 2756 (1981).
[9] S. M. Arakelyan, A. S. Karayan, and Y. S. Chilingaryan, Sov. Phys.-Dokl. **29**, 202 (1984) [Dokl. Akad. Nauk SSSR **275** 52 (1984)].
[10] G. Napoli, J. Phys. A: Math. Gen. **39**, 11 (2006).
[11] E. Guyon, Am. J. Phys **43**, 877 (1975).
[12] A. Y. Val'kov, E. V. Aksenova, and V. P. Romanov, Phys. Rev. E **87**, 022508 (2013).
[13] Á. Buka and N. Éber, eds., *Flexoelectricity in Liquid Crystals: Theory, Experiments and Applications* (Imperial College Press, London, 2012).
[14] A. J. Davidson and N. J. Mottram, Phys. Rev. E **65**, 051710 (2002).
[15] L. A. Parry-Jones, R. B. Meyer, and S. J. Elston, J. Appl. Phys. **106**, 014510 (2009).
[16] L. J. Cummings, C. Cai, and L. Kondic, J. Eng. Math. **80**, 21 (2013).
[17] C. V. Brown and N. J. Mottram, Phys. Rev. E **68**, 031702 (2003).
[18] A. A. T. Smith, C. V. Brown, and N. J. Mottram, Phys. Rev. E **75**, 041704 (2007).
[19] E. Mema, L. Kondic, and L. J. Cummings, Phys. Rev. E **95**, 012701 (2017).
[20] R. Stannarius, *Handbook of Liquid Crystals, Low Molecular Weight Liquid Crystals I: Calamitic Liquid Crystals* (Wiley, Weinheim, 2), Chap. III, 2.1.5., pp. 73–78.
[21] G. Barbero and L. R. Evangelista, *An Elementary Course on the Continuum Theory for Nematic Liquid Crystals*, Series on Liquid Crystals, Vol. 3 (World Scientific, Singapore, 2001).
[22] C. Oldano and G. Barbero, Phys. Lett. A **110**, 213 (1985).

[23] O. D. Lavrentovich, *The Oxford Handbook of Soft Condensed Matter* (Oxford University Press, Oxford, 2015), Chap. 3.3., pp. 111–116.

[24] L. D. Landau and E. M. Lifshitz, *Electrodynamics of Continuous Media*, 2nd ed., Course of theoretical physics, Vol. 8 (Butterworth-Heinemann, Oxford, 1984).

[25] V. A. Belyakov, I. W. Stewart, and M. A. Osipov, Phys. Rev. E **71**, 051708 (2005).

[26] R. P. Feynman, *Statistical Mechanics: A Set Of Lectures*, 2nd ed., Advanced Book Classics (Westview Press, New York, 1998).

[27] A. Y. Val'kov, V. P. Romanov, and M. V. Romanov, JETP **93**, 344 (2001).

[28] A. D. Kiselev, Phys. Rev. E **69**, 041701 (2004).

[29] L. D. Landau and E. M. Lifshitz, *Statistical Physics, Part 1*, 3rd ed., Course of Theoretical Physics, Vol. 5 (Butterworth-Heinemann, Oxford, 2000).